

## Four stages of pressure ridging

Mark A. Hopkins

U.S. Army Cold Regions Research and Engineering Laboratory, Hanover, New Hampshire

**Abstract.** The pressure ridging process is simulated using a two-dimensional particle model. Blocks are broken from an intact sheet of relatively thin lead ice pushed against a thick, multiyear floe at a constant speed. The blocks of ice rubble accumulate to form the ridge sail and keel. During the simulations the energy consumed in ridge growth, including dissipation, is explicitly calculated. On the basis of the results of simulations performed with the model, the ridging process can be divided into four distinct stages. The first stage begins with an intact sheet of lead ice impacting a floe and ends when the sail reaches its maximum height. In the second stage the ridge keel deepens and widens. The stage ends when the maximum keel draft is reached. In the third stage the direction of growth is leadward creating a rubble field of more or less uniform thickness. The third stage ends when the supply of thin ice is exhausted. In the fourth stage the rubble field is compressed between converging floes. The results of simulations establish the dependence of ridging energetics in the first and second stages on the thickness of the ice sheet and the amount of ice pushed into the ridge. The average profiles of the simulated ridges delineate the growth process in the first, second, and third stages. The energetics and profiles of the fourth stage were described by *Hopkins et al.* [1991]. Lead ice extents of up to 1300 m are pushed into ridges to determine maximum sail heights, keel drafts, and ridging forces.

### 1. Introduction

The variable thickness of the Arctic ice pack is created by deformation, which simultaneously causes formation of thick ice through ridge building and thin ice through lead creation. Since the energy expended in deformation is largely determined by the ridging process, an understanding of the energetics of pressure ridging is critical to the determination of ice strength on a geophysical scale [*Hopkins and Hibler*, 1989].

Pressure ridges are the piles of ice rubble that crisscross the Arctic ice pack, created from the rubble of ice broken during compressive deformation. The first computer model of the ridging process was developed by *Parmeter and Coon* [1972]. The simulations began with an ice sheet of uniform thickness. The motion of the rubble created by compression of the ice sheet was kinematically defined by various parameters. The simulations generated realistic ridge profiles, but to predict ridging forces, assumptions were needed as to the relationship between the potential energy of the ridge structure, which can be calculated from the ridge profiles, and energy dissipation, which was not modeled.

A two-dimensional dynamic model of the ridging process was developed by *Hopkins et al.* [1991]. This model, based on a particle simulation, considered the compression of a rubble-filled lead between multiyear floes. The ice rubble was modeled by a collection of rectangular pieces broken from a sheet of uniform thickness. Because the forces between individual ice pieces were explicitly calculated, it was possible to determine the fraction of the ridging work dissipated in frictional and inelastic contacts as well as the potential energy of the ridge structure.

*Hopkins* [1994] developed another dynamic model of pressure ridge formation, in which an intact ice sheet covering a refrozen lead was pushed at constant speed against a thick, multiyear floe. The thin sheet, breaking repeatedly in flexure, created the rubble blocks that form the ridge sail and keel. This study demonstrated the importance of friction as a dissipative mechanism. An equally interesting, but less obvious, finding was the role of friction in controlling the relative volumes of the ridge sail and keel. Because of the breadth of the parameter study, only 100 m of thin ice was pushed into each ridge.

The goal of the present study was to perform much longer simulations to determine the evolution of the ridge profile, ridging forces, and energetics as functions of lead ice thickness and the amount of lead ice pushed into the ridge. A part of this goal was the determination of maximum sail heights, keel drafts, and ridging forces. The evolution of the average ridge profiles, the forces, and the energetics obtained from the simulations suggested that the ridging process can be divided into four distinct stages. The first stage begins with an intact sheet of lead ice impacting a floe and ends when the sail reaches its maximum height. The second stage, in which the ridge keel grows wider and deeper, ends when the maximum keel draft is reached. The third stage, in which leadward growth creates a rubble field of more or less uniform thickness, ends when the supply of thin ice is exhausted. In the fourth stage the rubble field is compressed between converging floes.

The average profiles of the simulated ridges shown in Figures 3a–3c clearly delineate the growth process in the first, second, and third stages. The numerical results establish the dependence of ridging energetics in the first and second stages on the thickness of the ice sheet and the amount of ice pushed into the ridge. The transition in the ridging force between the first and second stages is clearly defined. The transition in the ridging force between the second and third stages cannot be detected in the current results. The profiles, forces, and energetics of the fourth stage, in which a rubble-filled lead is compressed between multiyear floes, described by *Hopkins et al.* [1991], are not discussed here.

This paper is not subject to U.S. copyright. Published in 1998 by the American Geophysical Union.

Paper number 98JC01257.

## 2. Dynamic Ridge Model

The pressure ridging model is based on a computer program that explicitly models the dynamics of a system of discrete, two-dimensional ice blocks. The position, orientation, velocity, and shape of each block are stored in arrays. At each time step the contact and body forces on each block are calculated and the blocks are moved to new locations with new velocities that depend on the resultant of the forces. The mechanical details of the model, which are the same as in the work by Hopkins [1994], are summarized here.

The important features of the ridging model are a dynamic, linear, viscous-elastic model of a floating ice sheet; flexural failure (including buckling) of the ice sheets; realistic block lengths broken from the parent sheet at points where tensile stress exceeds strength; secondary flexural breakage of rubble blocks; inelastic contacts between rubble blocks; frictional sliding contacts between blocks; separate friction coefficients for submerged and above water contacts; buoyancy of the ice sheets and rubble; and water drag. The key assumptions in this study are (1) the lead ice sheet breaks in flexure or by buckling and (2) the multiyear floe is capable of supporting any imbalance between sail and keel with minimal subsidence. Compressive failure is not considered.

The ridge model is based on a concept of ridge growth in which an intact sheet of thin lead ice of thickness  $h$  is driven against a thick, multiyear ice floe. A snapshot from a simulation is shown in Figure 1. The thin ice sheet, thick floe, and rubble blocks, broken from the sheet, are each composed of single rows of uniform, rectangular blocks that are attached to neighboring blocks by viscous-elastic joints. The discretization of the sheet, floe, and rubble blocks is shown in Figure 2 [Hopkins, 1994]. The skeletal layer, block beveling, and boundary conditions on the sheet and floe, shown in Figure 2, are discussed by Hopkins [1994]. Relative displacements between adjacent component blocks create forces and moments, internal to the sheet and rubble blocks. The internal forces on the component blocks are added to external forces exerted by the surrounding ice rubble, gravity, buoyancy, and boundary conditions.

The lead ice sheet may fail either through flexure or buckling. Flexural failure is caused by loads applied perpendicular to the neutral axis of the sheet, while buckling is caused by loads applied parallel to the axis. The deformation of the sheet necessary to create the instability that precedes buckling may result from an axial force being applied off the neutral axis or from unevenly distributed forces perpendicular to the axis, such as those that occur when the sheet overrides the rubble accumulation in front of the floe. The impor-

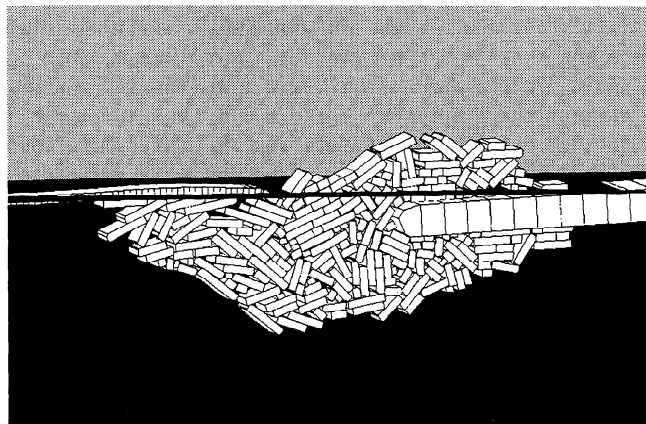


**Figure 1.** Snapshot from a ridging simulation at a point when a 150 m extent of 500 mm thick lead ice has been pushed into a 2 m thick floe.

tant point is that flexure and buckling failure occur because of dynamic effects and are not due to the imposition of any arbitrary criteria. The actual fracture of the sheet occurs when tensile stress from flexure or buckling exceeds the tensile strength. When the tensile stress in a joint at either surface of the sheet, floe, or a rubble block exceeds the specified strength, a crack is initiated. The crack propagates at constant speed (10 m/s) across the joint, requiring many time steps  $\Delta t \sim O(10^{-3} \text{ s})$  for completion. The block created by the fracture becomes part of the rubble and is added to the ridge structure. While the cracks must occur at joints, the length of the rubble blocks is variable since the blocks may contain any number of component blocks. The multiyear floe is modeled in a similar manner except that the floe breaks only in flexure. A broken joint between component blocks in the floe is hinged at the bottom of the floe as shown at point C in Figure 2. Any isostatic imbalance caused by the sail and keel is supported by spring and dashpots attached to the floe as shown in Figure 2.

Contact forces between rubble blocks, between rubble and sheet or floe, or between sheet and floe use a different force model that supports no tensile force. Two blocks are defined to be in contact if the polygons defining their shapes intersect. The force between two intersecting blocks is calculated in a local coordinate frame with axes normal and tangential to a contact surface connecting the intersection points. The force acts at the centroid of the area of intersection. A viscous-elastic normal force model is used with a Coulomb friction, tangential force model. The internal forces and moments at each joint in the ice sheet, floe, and rubble blocks and the external, contact forces between blocks are calculated at each time step. Equations of motion, derived from a Taylor series expansion about the current time, are integrated to find the updated positions and velocities.

The energetics of the simulations include the ridge building work, the potential energy of the ridge structure, the frictional dissipation, and inelastic dissipation. The ridge building force is the sum of the horizontal forces exerted on the thin ice sheet by the rubble. A force sufficient to push the lead ice sheet at a constant speed is assumed to be available. The rate of work is the product of the ridging force and the ice sheet velocity. The equations used to calculate the various energetic mechanisms are described by Hopkins [1994]. The components of the energy budget are measured in watts per meter of ridge width. Other energy sinks are translational and rotational kinetic energy, water drag, and viscous boundary forces (shown in Figure 2), which, in total, typically amount to less than 5% of the energy consumed. Ridging work is compared to the sum of the potential energy, kinetic energy, and dissipation terms to gauge the numerical accuracy of the simulation. In the simulations discussed below, the error in the energy balance was less than 1%.

## 3. Simulations of the Pressure Ridging Process

A series of simulations were performed to determine the dependence of the ridge profile, ridge-building forces, and energetics on the thickness of the lead ice sheet and the extent of lead pushed into the ridge. The parameters used in the simulations are listed in Table 1.

The sensitivity of the simulation to the speed of the lead ice sheet, the friction coefficients, and the elastic moduli is summarized here. A comparison of results of simulations with ice sheet speeds of 62.5 and 250 mm/s showed little difference [Hopkins, 1994]. The speed used here, 250 mm/s, an order of magnitude greater than field values, is used to reduce computational time. A driving force sufficient to move the lead ice sheet is assumed to be available at all times. The friction coefficients used throughout this study, which are listed Table 1, produced realistic ridge profiles in the study of Hopkins

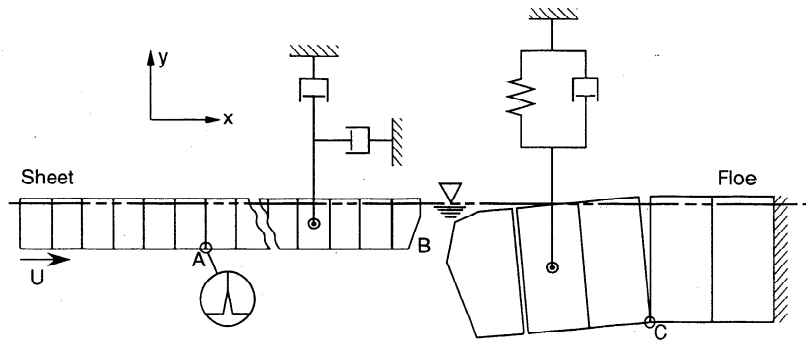


**Figure 2.** Discretization of the floe and lead ice sheet into uniform rectangular blocks; showing the boundary conditions on the lead ice sheet and floe. A skeletal layer is modeled by terminating the viscous-elastic joint between adjacent blocks (point A). The tip of the sheet is beveled (point B) to facilitate the sheet riding up the floe or over rubble blocks. The pin joint (point C) constrains the motion of a broken floe.

[1994]. The normal contact stiffness  $k_{ne}$  was set to an arbitrarily high value to make the overlap area in contacts between rubble blocks negligibly small. For typical contact forces in the range 1–10 kN, overlap areas range from  $10^{-5}$  to  $10^{-4}$  m<sup>2</sup>. The tangential stiffness coefficient in rubble contacts  $k_{te}$  was 60% of the normal value. The normal viscosity coefficient  $k_{nv}$  was set to 50% of the critical damping value  $2(k_{ne} h p_i)^{1/2}$  to produce highly inelastic behavior.

The elastic modulus  $E$  used for the lead ice, 100 MPa, is much smaller than the values of 1–2 GPa cited [Mellor, 1986] for young, saline ice. This low value was chosen in the early days of this project to minimize the brittle behavior of the model ice sheet. With realistic values of  $E$ , the lead ice tends to fail prematurely in the lead ahead of the floe rather than piling on the floe and pushing a train of blocks up the sail as shown in Figure 1. Therefore  $E$  was reduced until the ice sheet behaved in a less brittle manner, characterized by the ability of the sheet to pile blocks on the floe and push a train of

blocks up the sail. The brittle behavior of the model ice sheet has several causes. The first is the simplicity of the fracture model. The sheet is not capable of sustaining partial damage through micro-cracking. Once a crack is initiated, it travels completely through the sheet. The second reason is the two-dimensionality of the sheet. Once a crack is formed, there is little continuity between the two blocks. A real ice sheet is able to maintain continuity despite the presence of flexural cracks. This is probably due to the nonuniformity of the surface along the crack in the third dimension. The consequences of this reduction in the modulus  $E$  are discussed below.

Ten simulations were performed with each thickness of lead ice. A random variation ( $\pm 1\%$ ) in the elastic modulus at each joint in the lead ice sheet was used to create unique outcomes in simulations using the same initial configuration of ice and the same set of parameters. This small variation was sufficient to cause the simulations to diverge noticeably by the time several blocks had been broken

**Table 1.** Parameters Used in the Simulations

Parameter	Value
Lead ice thickness, $h$ , mm	400,500,600,700,800,900,1000
Floe thickness, m	
for $h = 400,500,600,700$ mm	2
for $h = 800$ mm	2,2.5,3,3.5
for $h = 900,1000$ mm	3.5
Lead ice speed, mm/s	250
Sheet block width, $W$	$1/8$ of characteristic length
Skeletal layer	$1/10$ of thickness to maximum of 60 mm
Elastic moduli	
floe top, GPa	1.0
floe bottom, GPa	0.67
lead ice top, MPa	100
lead ice bottom, MPa	67
Poisson's ratio, $\nu$	0.3
Tensile strength (ice top), kPa	750
Tensile strength (ice bottom), kPa	350
Ice density, $\rho_i$ , kg /m <sup>3</sup>	920
Water density, $\rho_w$ , kg /m <sup>3</sup>	1010
Dry friction, $\mu$	1.0
Wet friction, $\mu_w$	0.6
Normal contact stiffness, $k_{ne}$ , N/m <sup>3</sup>	$10^8$

from the parent sheet. This does not imply extreme sensitivity to the elastic modulus but, rather, the chaotic nature of the ridging process.

#### 4. Ridge Profiles

The ridging simulations begin with an intact sheet of lead ice pushed against a thick, multiyear ice floe at a constant speed. As the ice sheet collides with the floe, it fails, either in flexure or by buckling, creating rubble blocks that accumulate to form the ridge structure. Sail growth takes place by direct piling of blocks pushed by the sheet onto the floe. The blocks, broken in succession from the sheet, form a train climbing the leadward side of the sail. The force required to push the blocks depends on the height and slope of the sail and the friction between sliding blocks. The part of the ridge keel that is in front of the floe, at the water surface, functions as a platform supporting the downward component of the sail building force [Hopkins, 1994]. Sail growth continues as long as the sheet is able to transmit the force and the platform is able to support the downward component. If the sheet is unable to transmit the force, it buckles. If the platform is unable to support the force, it collapses, becoming enlarged in the process. Early ridge growth exhibits a cyclic alternation between sail growth and platform growth.

Rubble is added to the keel at the water surface when the progress of the sheet, sliding across the platform, is obstructed, causing it to buckle or break in flexure. Rubble is also added to the keel when blocks piled on the leadward slope of the sail become unstable and collapse into the platform. As the keel grows, it spreads in both directions. The spreading keel is continually pushed in the direction of the floe by the motion of the sheet. Pressure on the ice rubble forming the keel, caught between the oncoming lead ice and the floe, causes the keel to deepen and pushes rubble beneath the floe. Since

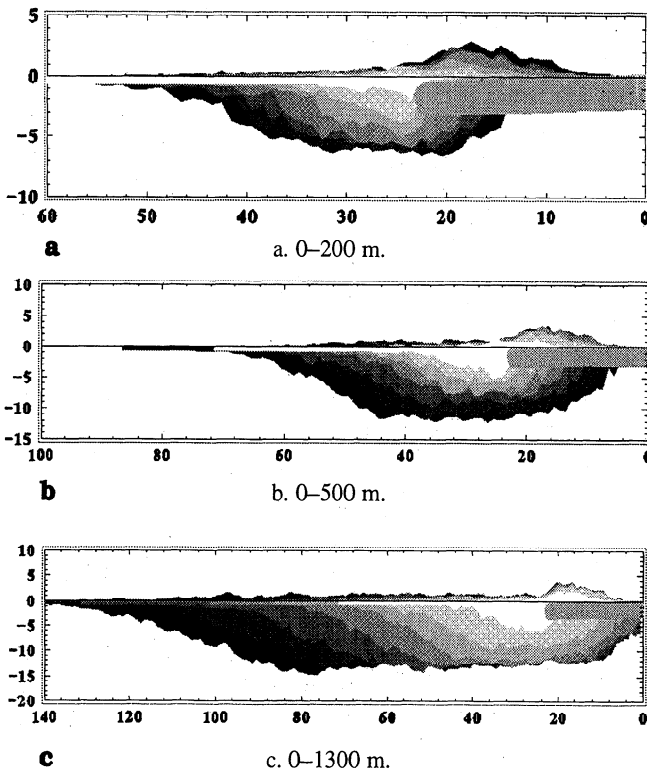


**Figure 3.** Evolution of the average ridge profile for lead ice extent. Successive profiles are denoted by darkening shades of gray. Profiles are averages of 10 simulations using 900 mm thick lead ice and a 3.5 m thick floe.

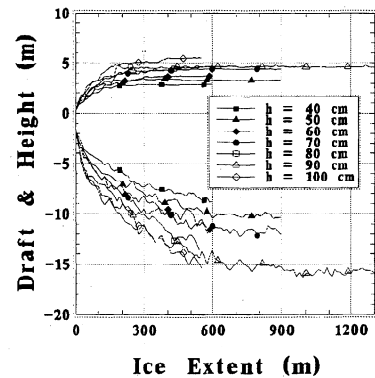


**Figure 4.** Evolution of the average sail height and keel draft from simulations as a function of the extent of lead ice pushed into the ridge.

this force must be transmitted through the lead ice, both the maximum sail height and keel draft depend on the strength of the lead ice.

The evolution of the average ridge profile in simulations using 900 mm thick lead ice and a 3.5 m thick floe is shown in Figures 3a–c. Profiles were obtained at uniform intervals during simulations by dividing a ridge cross section into 250 mm wide vertical strips. The maximum elevation and draft of the ice in each strip were determined. Average ridge profiles were obtained by averaging profiles from 10 simulations. Figure 3a shows the growth in the average profile over an interval from the beginning to the point where 200 m of lead ice had been pushed into the ridge, a period in which both the sail and keel are growing and which roughly corresponds to stage 1. In Figure 3b, 500 m of ice has been pushed into the ridge, the ridge keel has grown 5.5 m deeper, while the sail is essentially unchanged. This period corresponds to stage 2. In Figure 3c, 1300 m of ice has been pushed into the ridge. This period, in which growth is leadward, corresponds to stage 3.

The evolution of the average maximum sail height and keel depth as a function of the extent of lead ice pushed into the ridge is shown in Figure 4. The average maximum sail height and keel depth were obtained by averaging the maximum sail height and keel depth from each of 10 simulations at each time. Maximum sail height is reached at about 200 m of lead ice extent, regardless of thickness. Maximum keel draft was reached in the simulations with 500, 700, and 900 mm thick ice. The simulations with 400, 600, 800, and 1000 mm thick ice were terminated at the points shown in Figure 4 before maximum keel draft was reached. During periods of growth, sail height and keel draft appear to increase with the square root of ice extent. The maximum sail heights and keel drafts obtained with each ice thickness are shown in Figure 5. The brackets on the data points show standard deviation. The solid line in Figure 5 shows the upper bound on sail height  $H = 5.24h^{0.5}$  from Tucker *et al.* [1984]. The dotted line shows the upper bound on keel draft given by  $D = 15.2h^{0.5}$  from Melling and Riedel [1996].

The maximum sail height, shown in Figure 5, is proportional to  $h^{1/2}$ . This relationship can be derived for limit height ridges from the following chain of reasoning. The volume of lead ice in a ridge is the product of ice thickness  $h$  and the extent of lead ice pushed into the ridge  $L$ . The lead ice extent required to reach maximum sail height  $L_I$  (defined by (5)) is independent of thickness. Since sail height is proportional to the square root of ice volume, it follows that maximum sail height is proportional to  $h^{1/2}$ . However, the dependence of sail height on the square root of ice thickness does not, in

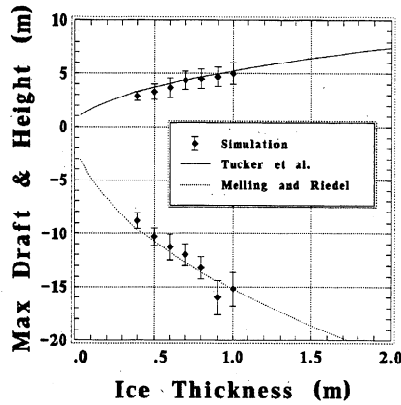


Figure 5. Maximum average sail heights and keel drafts from simulations compared with the limiting sail height envelope obtained by Tucker et al. [1984] and the limiting keel draft envelope obtained by Melling and Riedel [1996].

and of itself, imply limiting behavior. Such dependence would also be found if, following Hibler [1980], the amount of lead ice pushed into a ridge is simply uncorrelated with thickness. Here it is helpful to remember that, in the central pack, ridges do not grow in isolation. The deformation at one point is a function of the deformation in the surrounding pack, such that a thin, weak ice parcel may ridge less than a nearby parcel that is thicker and stronger.

5. Energetics of Pressure Ridging

The ridge-building force, the total energy consumed, the potential energy of the ridge structure, and the energy lost to frictional and inelastic dissipation are calculated at each time step during the simulations. The variation of the ridge-building force during a simulation using 900 mm lead ice is shown in Figures 6a and 6b. The force was stored at 0.2 s intervals. Peak ridging forces accompany buckling of the lead ice sheet. The buckling force, assuming an unconfined beam end [Kovacs and Sodhi, 1980], is approximately

$$P = \rho_w g L_c^2 \tag{1}$$

where  $L_c$  is the characteristic length given by

$$L_c = (Eh^3 / 12\rho_w g)^{1/4} \tag{2}$$

The characteristic length for 900 mm thick ice using the parameters given above ( $E = 100$  MPa) is 4.98 m. This yields a buckling force of 245 kN/m, which is close to the peak forces in Figures 6a and 6b.

During the sail-building period, the ridging force is determined by the amount of force needed to enlarge the sail. The oncoming lead ice sheet enlarges the sail by pushing a train of blocks up the leadward slope of the sail. The ridging force  $F$  is determined by the weight of the train of blocks, which is proportional to the thickness of the lead ice  $h$  times the length of the block train  $l$  ( $F \propto hl$ ). The length of the block train is proportional to the sail height, which is, in turn, proportional to the square root of the sail volume  $V$  ( $l \propto V^{1/2}$ ). Assuming that the sail porosity remains relatively constant and that the ridge profile evolves in a self-similar fashion (as it does in Figure 3a), then the sail volume is proportional to the product of ice thickness and the extent  $L$  of lead ice pushed into the ridge ( $V \propto hL$ ). Thus in the first stage of ridging, while sail growth is occurring, the average ridging force is given by

$$F = ah^{3/2}L^{1/2} \tag{3}$$

where  $a$  is a constant to be determined. After the sail reaches its maximum height, the ridging force is assumed to be limited by the buckling of the lead ice, as appears to be the case in Figures 6a and 6b. Thus, using (1) and (2), in the stages following sail building, the average ridging force is given by

$$F = bh^{3/2} \tag{4}$$

where  $b$  is also a constant to be determined. The sail reaches its maximum height when the sail building force equation (3) reaches the force determined by the buckling limit equation (4). Setting (3) equal to (4), I find that the extent of lead ice needed to reach a maximum sail height  $L_I$  is independent of thickness and is given by

$$L_I = \left(\frac{b}{a}\right)^2 \tag{5}$$

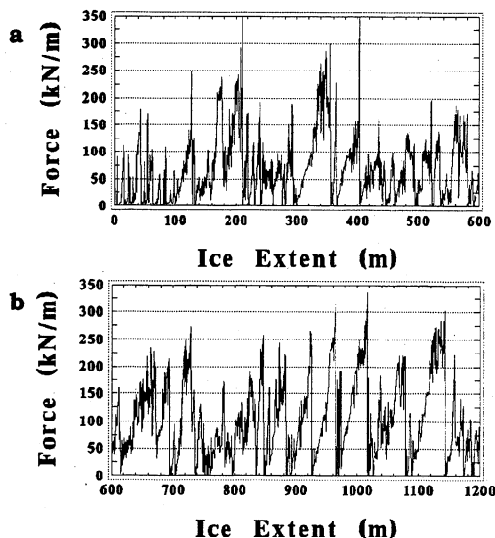


Figure 6. Instantaneous ridge building force (kilonewtons per meter) versus extent of lead ice from a simulation using 900 mm thick lead ice.

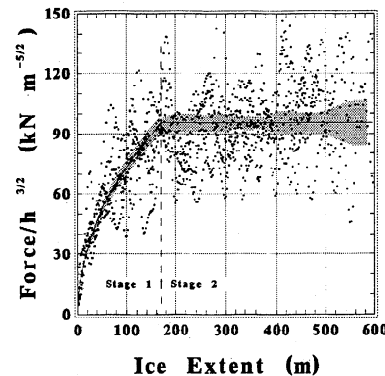


Figure 7. Average ridging force (kilonewtons per meter) divided by thickness of the lead ice  $h^{3/2}$  versus extent of lead ice. Equations (6) and (7) are plotted as a solid line within the stippled area, which defines a 95% confidence interval. The point data are the averaged and smoothed results of 10 simulations with each ice thickness.

Although surprising, this result is clearly indicated in Figure 4. The extent of lead ice needed to reach maximum keel draft also appears to be independent of ice thickness in Figure 4, but no equation for the extent, analogous to (5), is apparent.

The constants  $a$  and  $b$  were calculated from the ridging forces stored at 0.2 s intervals during the simulations using a least squares regression. The constant  $a$ , from a graph of  $F/h^{3/2}$  versus  $L$  using (3) for  $L < 150$  m, was 7300. Similarly, the constant  $b$  from (4) for  $L > 220$  m was 95,400. Using these values of  $a$  and  $b$ , the lead ice extent  $L_I$  required to reach maximum sail height equation (5) is 170.7 m and the average ridging force in newtons per meter is

$$F = 7300h^{3/2}L^{1/2} \quad L \leq L_I \quad (6)$$

$$F = 95,400h^{3/2} \quad L > L_I \quad (7)$$

The average ridging force, divided by  $h^{3/2}$ , is shown in Figure 7. Equations 6 and 7 are plotted as a solid line within the stippled area, which defines a 95% confidence interval. The point data in Figure 7 show the averaged and smoothed results of 10 simulations with each ice thickness. The transition from stage 1 forces equation (6) to stage 2 forces equation (7) is delineated by the vertical dashed line in Figure 7. The buckling force shown in (1), using the parameter values given in Table 1, is  $287 h^{3/2}$ . Thus the peak average ridging force in (7) is approximately  $1/3$  of the buckling force. This relationship follows from the force record, which is characterized by periods of linear increase until the force reaches the buckling limit, followed by an abrupt drop to zero as shown in Figure 6b.

Equations can be derived for the ridging work by expressing the rate of work in terms of force as,  $dW/dt = uF$ , replacing the lead ice velocity  $u$  by the time derivative of the lead ice extent  $dL/dt$  and integrating. Using (6) and (7) for the ridging force, ridge-building work in joules per meter is given by

$$W = 4867h^{3/2}L^{3/2} \quad L \leq L_I \quad (8)$$

$$W = 4867h^{3/2}L_I^{3/2} + 95,400h^{3/2}(L - L_I) \quad L > L_I \quad (9)$$

The energy consumed in the ridging process (megajoules per meter), divided by  $h^{3/2}$ , as a function of the extent of lead ice, is shown in Figure 8. The results are the averages of 10 simulations with each ice thickness. Equations (8) and (9) are plotted as a solid line through the data. The energy consumed by the ridging process

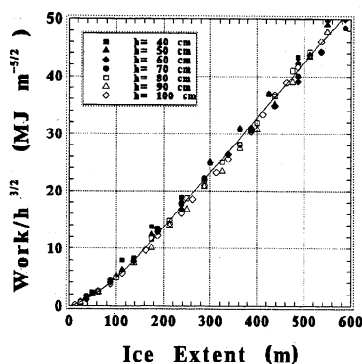


**Figure 8.** Ridging work (megajoules per meter) divided by  $h^{3/2}$  versus extent of lead ice from the averaged results of sets of 10 simulations with each thickness of lead ice. Equations (8) and (9) are plotted as a solid line through the data.

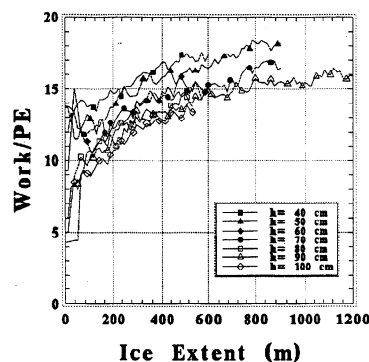


**Figure 9.** Ratio of ridging work to potential energy versus extent of lead ice from the averaged results of sets of 10 simulations with lead ice of several thicknesses.

is stored in the potential energy of the ridge structure and dissipated by frictional and inelastic contacts. Similar equations for the frictional dissipation  $\Phi_f$ , inelastic dissipation  $\Phi_i$ , and the change in the potential energy of the ridge structure  $\Delta PE$  are given in the appendix.

The ratio of work to potential energy is an important variable in large-scale sea ice models [Hibler, 1980; Flato and Hibler, 1995], where it is used to parameterize total energy losses in terms of the change in potential energy due to ridging. The ratio of work to potential energy, expressed as a function of the extent of lead ice pushed into the ridge, is shown in Figure 9. The ratio, which increases steadily with lead ice extent, also appears to be inversely related to lead ice thickness. In the longest running simulations, using 900 mm thick lead ice, the ratio seems to level out. This leveling out may indicate the transition to stage 3 of the ridging process. It is interesting to note that Flato [1991], in sensitivity tests with a large-scale sea ice model, found that a ratio of 14 gave the best agreement with buoy drift data.

Increasing floe thickness might be expected to affect the ridging process by more strongly impeding the progress of the thin ice sheet. The effect of variation of floe thickness on the evolution of the ridge profile is shown in Figure 10. The simulations used 800 mm thick lead ice. Since sail height and keel depth are determined by the buckling strength of the thin ice sheet, variation of the floe thickness, within the range tested, had no appreciable effect. Nor did floe thickness have any significant effect on the energetics. Support for the isostatic imbalance of the ridge structure was not an issue because the boundary conditions imposed upon a floe allow it to support any imbalance.

## 6. Discussion

The results outlined above may be summarized as follows. During the initial period of ridge growth the size of the sail increases and the average force required to enlarge it (6) grows as well. Sail growth stops when the force, which the lead ice sheet must exert to push additional ice onto the sail, exceeds the buckling strength of the sheet. The maximum average ridging force in (7) is approximately  $1/3$  of the buckling force in (1) owing to the linear increase of the force to the buckling limit as shown in Figures 6a and 6b. The extent of lead ice necessary to reach maximum sail height (5), found by equating the expressions for the average ridging force during the period of sail growth (3) and the maximum ridging force (4), was independent of ice thickness. The maximum average ridging force, the maximum sail height and keel depth, and the extent of lead ice

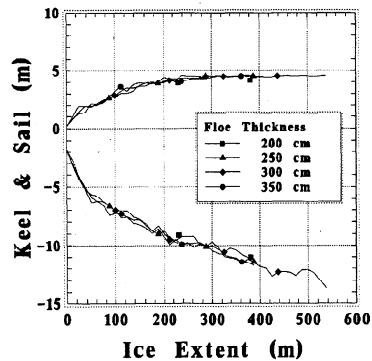


**Figure 10.** Comparison of the average sail height and keel draft for four floe thicknesses. Lead ice thickness is 800 mm.

needed to reach maximum sail height depend on the buckling strength. It is again worth emphasizing that buckling of the thin ice sheet in the simulations is a dynamic process and not due to the imposition of any arbitrary criteria such as (1).

The buckling strength of the lead ice sheet, nominally given by (1), depends on the square root of the elastic modulus. As discussed above it was necessary to use a modulus of 100 MPa to minimize the brittle behavior of the model ice sheet. By minimizing brittle behavior, the ice sheet was able to pass over the ice rubble floating in front of the floe without falling apart owing to multiple flexural failures. Lead ice sheets with moduli greater than 100 MPa generally failed to such a degree while traversing the floating rubble that they were unable to create realistic sails. The elastic modulus of 100 MPa used in the simulations is at least an order of magnitude below values typically cited for young, saline ice [Mellor, 1980]. If it were possible to use a nonbrittle ice sheet with a more realistic modulus in the simulations, then one would logically expect the maximum ridging force denoted in (7) and sail height, which depend on the buckling strength shown in (1), to scale by the square root of the increase in the modulus. A modulus of 1 GPa would increase the maximum ridging force and sail height found in this study by a factor of the square root of 10. The extent of ice needed to reach maximum sail height  $L_f$  (5) would increase by a factor of 10 to about 1.7 km. The average ridging force (6 and 7), plotted in Figure 7, would be capped at a level of about 300 kN/m for 1 m thick ice. The range of maximum sail heights shown in Figure 5 (from the simulations) would increase by the square root of 10 from 3–5 to 9–16 m.

This train of reasoning leads to the interesting question of whether the field measurements of Tucker *et al.* [1984] and Melling and Riedel [1996] in Figure 5 represent the maximum possible sail heights and keel drafts or just the maximums found in that region of the Arctic. Sail height and keel draft can also be limited by available forces and lead widths. It is possible that the driving forces in the central Arctic are insufficient to create limit ridge sails and keels. Increasing the maximum average ridging force in (7) by a factor of the square root of 10, consistent with a 1 GPa modulus, gives a maximum average ridging force of 300 kN/m for 1 m thick ice with peak forces of 900 kN/m. The forces measured by Richter-Menge and Elder [this issue] in the Beaufort Sea, during a 6 month period extending through the winter, were in the 50 to 100 kN/m range with peaks of 200–400 kN/m. This range of forces agrees quite well with the forces in Figure 7, which produced the sail heights and keel drafts in good agreement with field measurements shown in Figure 5. Thus it is possible that the maximum sail heights and keel drafts measured by Tucker *et al.* [1984] and Melling and Riedel [1996] were limited by the available driving forces.

One place where limited height sails are likely to be found is in onshore pileups. Onshore ice pileup is similar to the pressure ridging process. In both processes a sheet of intact ice is pushed up a pile of ice rubble and the height of the pile is limited by the strength of the ice sheet. The fact that one is grounded and the other is floating does not affect the force needed to pile ice up to a given height. In other words it takes the same force to push blocks up a 10 m ridge sail as it does to push blocks of the same thickness up a 10 m pileup. Kovacs and Sodhi [1980] give an extensive catalog of reports of shore ice pileup events. The events from their work which listed parent ice thickness and pileup height, along with two more recent events, are summarized in Table 2.

All of the events in Table 2 are 2–4 times higher than sail heights given in Figure 5 for the same ice thickness. The last event in Table 2, which occurred on the eastern side of the Gulf of Bothnia, early in the winter of 1996, is especially pertinent in that it was an obvious case of limiting behavior. This was evident from the plateau-like structure of the pileup, which consisted of many peaks of similar height extending 20–30 m in the direction from which the parent ice sheet came and several hundred meters in the transverse direction.

On the basis of the pileup events listed in Table 2, it is probable that the maximum sail heights and keel drafts measured by Tucker *et al.* [1984] and Melling and Riedel [1996] do not represent the maximum possible heights and drafts but, instead, represent maxima dictated by available driving forces or perhaps available lead ice extent. In this case the agreement between the simulation results and the field measurements in Figure 5 probably depends on the rough agreement between the force levels found in the simulations and in the field.

The conclusion that limit ridge sails are rare in the central Arctic is certainly not the only possible explanation for the question posed by Figure 5. One alternative is that true ridging forces are much higher than those predicted by the simulations. This would permit limit sail heights similar to those measured by Tucker *et al.* [1984] to coexist with buckling strength limitations corresponding to realistic moduli. The problem with this explanation is that, with ridge size fixed, the ratio of work to potential energy would increase with the ridging forces. A significantly larger ratio than the 10–18 found in this study would probably result in total stoppage of circulation in the Arctic in winter. Another alternative is that true ridging forces are much lower than those predicted by the simulations. However, this requires one to discard the assumption that the ridging force is limited by the buckling strength of the thin ice sheet. Yet a third alternative is that limit sail heights are never reached because the multiyear floes on which the ridges are built cannot support them. The present model assumes that the floe, even though broken, is capable of supporting any imbalance caused by a large sail.

**Table 2.** Data From Shore Ice Pileup Events

$h$ , m	$H$ , m	Source
NA	22.0	Kovacs and Sodhi [1980], p. 217
0.25	6.0	Kovacs and Sodhi [1980], p. 222
0.51	12.0	Kovacs and Sodhi [1980], p. 222
0.60	13.3	Kovacs and Sodhi [1980], p. 222
1–2	15.0	Kovacs and Sodhi [1980], p. 237
0.90	10.0	Kovacs and Sodhi [1980], p. 250
0.75	14.0	Alestalo <i>et al.</i> [1986]
0.08	3.0	P. Kankaanpaa and Z. Zhang [1997]

Abbreviations are  $h$ , ice thickness and  $H$ , sail height.

It is unlikely that the ridging forces found in the simulations are wildly wrong. The simulation results and the sail and keel data from field measurements shown in Figure 5 have the same envelope, and the ridging forces fall into the same range as the field measurements of *Richter-Menge and Elder* [this issue]. In addition, a comparison of the results of simulations of ice pileup on a ramp, using the same computer model used in this study, with similar experiments performed in the Cold Regions Research and Engineering Laboratory ice basin found that the simulation forces underestimated the model forces by only 20% [Hopkins, 1997].

## 7. Conclusions

A computer model of the pressure ridging process has been developed in which a sheet of thin lead ice is pushed against a thick multiyear floe at constant speed. Blocks of ice broken from the sheet accumulate to form the ridge sail and keel. The model is based on the assumption that sail growth and keel growth are ultimately limited by the buckling strength of the lead ice sheet, which must transmit the ridge building force. Simulations performed with ice sheets of various thicknesses were used to determine the dependence of the ridging force, the sail height and keel draft, and the ratio of ridging work to potential energy on the extent of lead ice pushed into the ridge.

On the basis of the simulation results, it is possible to divide the ridging process into four distinct stages. The first stage begins with an intact sheet of lead ice impacting a floe and ends when the maximum sail volume is reached. In the second stage the ridge keel deepens and broadens. The second stage ends when the maximum keel draft is reached. In the third stage the direction of growth is leadward, creating a rubble field of more or less uniform thickness. The third stage ends when the intact sheet of lead ice is consumed. The fourth stage is the compression of the rubble field between floes. Of course, ridge growth can end at any point in the process if driving forces become insufficient or the supply of lead ice is exhausted.

In the first stage the average ridging force, which increases with sail height, is proportional to ice thickness to the  $3/2$  power times the square root of the extent of lead ice pushed into the ridge. The duration of the first stage, in terms of the extent of lead ice, is independent of lead ice thickness. Maximum sail height is proportional to the square root of the lead ice thickness. Both the ridging force and sail growth are limited by the force required to cause the lead ice sheet to buckle. Keel growth during the first stage must be sufficient for the platform, the part of the keel at the water surface in front of the floe, to support the downward component of the sail-building force. The ratio of work to potential energy increases steadily during the first stage.

In the second stage the average ridging force is constant, is proportional to ice thickness to the  $3/2$  power, and is approximately  $1/3$  of the buckling strength of the lead ice sheet. Ridge growth is downward. Rubble is added to the keel at the surface of the ridge platform. The keel deepens by compression between the lead ice sheet and the floe. Compression also drives the keel rubble under the floe. The keel draft increases until the force required to further compress the floating rubble in the keel equals the buckling strength of the lead ice. The ratio of work to potential energy continues to increase, albeit more slowly, during the second stage.

In the third stage the ridging force remains constant, approximately  $1/3$  of the buckling force. Ridge growth is leadward, leading to the formation of a rubble field of roughly uniform thickness. The thickness or draft of the rubble field is dictated by the limit imposed on the force required to compress the floating rubble by the buckling strength of the lead ice sheet. The ratio of work to potential energy appears to be constant during the third stage.

In the fourth stage, which was not addressed in this study, the rubble field is compressed between converging floes. The force resisting compression is proportional to the square of the thickness or draft of the floating rubble. The force is limited only by the buckling strength of the floes. Results of simulations of this type of ridging are described by *Hopkins et al.* [1991].

The transition from the first stage to the second stage, which terminates sail growth, and from the second stage to the third stage, which terminates keel growth, are determined by the buckling strength of the lead ice sheet. Thus the maximum ridging force, sail height, and keel draft depend on the buckling strength. The estimates of these quantities found in this study depend on a modulus of elasticity for the model ice sheet used in the ridging simulations that is at least an order of magnitude below typical estimates. The low modulus was necessitated by the simplicity of the model of the lead ice sheet. If the maximum forces, sail heights, and keel drafts predicted by the simulations are extrapolated to account for a more realistic modulus, then it appears likely that ridges in the central Arctic will rarely ever reach the second stage. If this is the case, then it is likely that the second, third, and fourth stages of the ridging process will be only found in the proximity of land where, indeed, the highest ice pileups and largest rubble fields are found.

## Appendix

Equations for the various components of the energy budget obtained from a least squares fit to the data are given herein. The frictional dissipation  $\Phi_f$  in watts per meter, is

$$\Phi_f = 3885h^{3/2}L^{3/2} \quad L \leq L_I \quad (A1)$$

$$\Phi_f = 3885h^{3/2}L_I^{3/2} + 80,780h^{3/2}(L - L_I) \quad L > L_I \quad (A2)$$

The energy dissipated by inelastic contacts  $\Phi_i$ , in watts per meter, is

$$\Phi_i = 560h^{3/2}L^{3/2} \quad L \leq L_I \quad (A3)$$

$$\Phi_i = 560h^{3/2}L_I^{3/2} + 5741h^{3/2}(L - L_I) \quad L > L_I \quad (A4)$$

The change in the potential energy of the ridge structure  $\Delta PE$ , in watts per meter, is

$$\Delta PE = 450h^{3/2}L^{3/2} \quad L \leq L_I \quad (A5)$$

$$\Delta PE = 450h^{3/2}L_I^{3/2} + 5708h^{3/2}(L - L_I) \quad L > L_I \quad (A6)$$

**Acknowledgments.** The author thanks the Office of Naval Research for the opportunity to do this work. The author also thanks Walter Tucker III and Jackie Richter-Menge for their valuable criticism and advice, which improved this manuscript.

## References

- Alestalo, J., O. Heikkinen, and H. Tabuchi, Sea ice deformation in the Bothnian Bay off Hailuoto, Finland, in March 1986, *Bothnian Bay Reports*, edited by O. Timola, Perameri Res. Stn., Univ. of Oulu, Oulu, Finland, 1986.
- Flato, G.M., Numerical investigation of the dynamics of a variable thickness Arctic ice cover, Ph.D. thesis, Thayer School of Engineering, Dartmouth Coll., Hanover, N.H., 1991.
- Flato, G.M., and W.D. Hibler, III, Ridging and strength in modeling the thickness distribution of Arctic sea ice, *J. Geophys. Res.*, 100, 18,611–18,626, 1995.

- Hibler, W.D., III, Design and maximum error estimation for small error low pass filters, *Res. Rep. 304*, Cold Reg. Res. and Eng., Hanover, N.H., 1972.
- Hibler, W.D., III, Modeling a variable thickness sea ice cover, *Mon. Weather Rev.*, 108, 1943–1973, 1980.
- Hopkins, M.A., On the ridging of intact lead ice, *J. Geophys. Res.*, 99, 16,351–16,360, 1994.
- Hopkins, M.A., Onshore ice pile-up: A comparison between experiments and simulations, *Cold Reg. Sci. and Technol.*, 26, 205–214, 1997.
- Hopkins, M.A., and W.D. Hibler III, On modeling the energetics of the ridging process, *Proceedings of the Eighth International Conference on Offshore Mechanics and Arctic Engineering IV*, edited by N.K. Sinha, D.S. Sodhi, and J.S. Chung, The Hague, Netherlands, American Society of Mechanical Engineers, 175–178, 1989.
- Hopkins, M.A., W.D. Hibler III, and G.M. Flato, On the numerical simulation of the sea ice ridging process, *J. Geophys. Res.*, 96, 4809–4820, 1991.
- Kankaanpää, P., and Z. Zhang, Morphology of a grounded ridge, in *ZIP-97 Data Report*, Report Series in Geophysics, 37, edited by J. Haapala and M. Leppäranta, University of Helsinki, Helsinki, 1997.
- Kovacs, A., and D.S. Sodhi, Shore ice pile-up and ride-up: Field observations, models, theoretical analyses, *Cold Reg. Sci. and Technol.*, 2, 209–288, 1980.
- Melling, H., and D.A. Riedel, Development of seasonal pack ice in the Beaufort Sea during the winter of 1991–1992: A view from below, *J. Geophys. Res.*, 101, 11975–11992, 1996.
- Mellor, M., Ship resistance in thick brash ice, *Cold Reg. Sci. and Technol.*, 3, 305–321, 1980.
- Mellor, M., Mechanical behavior of sea ice, in *The Geophysics of Sea Ice*, edited by N. Untersteiner, 165–281, Plenum, New York, 1986.
- Parmeter, R.R., and M.D. Coon, Models of pressure ridge formation in sea ice, *J. Geophys. Res.*, 77, 6565–6575, 1972.
- Richter-Menge, J.A., and B.C. Elder, Characteristics of pack ice stress in the Alaskan Beaufort Sea, *J. Geophys. Res.*, this issue.
- Tucker, W.B. III, D.S. Sodhi, and J.W. Govoni, Structure of first-year pressure ridge sails in the Prudhoe Bay region, *The Alaskan Beaufort Sea: Ecosystems and Environment*, edited by P.W. Barnes, D.M. Shell, and E. Reimnitz, pp. 115–135, Academic Press, San Diego, Calif., 1984.

---

M.A. Hopkins, U.S. Army Cold Regions Research and Engineering Laboratory, Hanover, New Hampshire (e-mail: hopkins@crrel.usace.army.mil)

(Received April 30, 1997; revised November 7, 1997; accepted April 17, 1998.)